Nanoscale

Accepted Manuscript

ROYAL SOCIETY OF CHEMISTRY

www.rsc.org/nanoscale

Nanoscale

Paper

Influence of Electron Storing, Transferring and Shuttling Assets of Reduced Graphene Oxide at the Interfacial Copper Doped TiO₂ p-n Hetero-junction for the Increased Hydrogen Production

Sundaram Ganesh Babu,[a] Ramalingam Vinoth,[a] Dharani Praveen Kumar,[b] Muthukonda V. Shankar,[b]

5 **Hung-Lung Chou,[c] Kizhanipuram Vinodgopal,[d],* and Bernaurdshaw Neppolian[a],***

Herein we report a simple, low-cost and scalable preparation of reduced graphene oxide (rGO) supported surfactant-free Cu_2O-TiO_2 nanocomposite photocatalysts by ultrasound assisted wet impregnation method.
10 Unlike the conventional preparation techniques, simultaneous reduction of Cu^{2+} (as in precursor) to Cu^+ (Cu_2O) and graphene oxide (GO) to rGO is achieved by ultrasonic method without addition of any external reducing agent which is ascertained by X-ray diffraction (XRD) and X-ray photoelectron spectroscopy (XPS) analyses. The UV-visible diffused reflectance spectroscopy (DRS) studies (Tauc plot) provide evidence that the loading of Cu_2O tailored the optical band gap of the photocatalyst from 3.21 eV
15 to 2.87 eV. The photoreactivity of the as-prepared Cu_2O-TiO_2/rGO samples is determined *via* H_2 evolution from water in presence of glycerol as a hole (h^+) scavenger under visible light irradiation. Very interestingly, the addition of rGO augments the carrier mobility at Cu_2O-TiO_2 p-n heterojunction which is manifest from the utterly reduced luminescence intensity of Cu_2O-TiO_2/rGO photocatalyst. Hence rGO astonishingly enhances the photocatalytic activity as compared with pristine TiO_2 nanoparticles (NPs) and
20 Cu_2O-TiO_2, by factors of ~14 and ~7, respectively. An utmost H_2 production rate of 110968 μmol h^{-1} g_{cat}^{-1} is obtained with a 1.0% Cu and 3.0% GO photocatalyst composition which is extremely superior than the previously reported graphene based photocatalysts. Besides, the present H_2 production rate is much higher than that of precious/noble metal (especially Pt) assisted (as co-catalyst) graphene based photocatalysts. Moreover, to the best of our knowledge, this is the highest H_2 production rate (110968
25 μmol h^{-1} g$_{cat}^{-1}$) by a graphene based photocatalyst through the splitting of water under visible light irradiation.

Introduction

The increasing energy demand and the undesirable environmental consequences arising from the burning of fossil fuels have led to
30 search for renewable and environmentally benign alternative energy recourses.[1—4] Owing to its high combustion energy and zero emission, hydrogen has always been a primary candidate as a potential fuel.[5—8] One of the best ways to produce H_2 from renewable sources is water splitting.[9,10] Honda and Fujishima first
35 reported the use of a TiO_2 electrode for water splitting in 1972.[11] Following this initial breakthrough, powdered photocatalysts and semiconductor photoelectrodes for water splitting have been extensively studied for renewable energy, applications, recycling polluted water or air, etc.[12—14] Among the existing methodologies
40 for H_2 generation, powdered-type photocatalysts are preferable because it requires only light source and a water pool containing photocatalyst powders. This system also offers an interesting opportunity to generate H_2 in a more energy-efficient manner in which the photo-excited electron-hole pairs can be generated by
45 simple electromagnetic irradiation with energy higher than that of

the band gap energy. The photogenerated electrons reduce H^+ ions in the aqueous solution to form H_2.[15—17] Several promising photocatalysts such as TiO_2,[18] Fe_3O_4,[19] $KNbO_3$ microcubes,[20] $NiO/NaTaO_3$,[21] Cu_2O,[22] GaN:ZnO,[23] $La_2Ti_2O_7$,[24] and $Sr_2Nb_2O_7$,[25]
50 have been identified. Nonetheless, the low efficiency of photocatalysis is due to competitive electron-hole recombination. This can be overcome by using efficient electron transport matrices, such as conductive polymer films or high-carrier migrant carbon nanostructures.[26,27] Since the delocalized
55 conjugated carbon materials like CNTs and graphene are well matched with the photocatalysts in energy level, an intensive interface hybrid effect emerges between these materials, thereby causing rapid charge separation and slow charge recombination in the electron-transfer process.[28] Furthermore, it tends to prevent
60 the aggregation of metal nanoparticles (MNPs) during the course of the reaction which is also a prime limitation in photocatalysis.[29] So the use of solid supports especially carbonaceous materials is finding greater application in water splitting reaction. For instance, Wang *et al.* proposed that the
65 photogenerated electrons in the space-charge regions may be

transferred into rGO, while the holes remain on the semiconductor (TiO_2) material, thus retarding the recombination of electrons and holes.[30] Similarly, Jia *et al.* proposed that N-doped graphene enhances the photocatalytic activity towards

5 water splitting under visible light illumination and they observed the relative order of reactivity for H_2 production was N-graphene/CdS > graphene/CdS > GO/CdS > CdS.[31]

Although the solid support matrices retard the electron-hole pair recombination, possess high carrier mobility and also prevent

10 aggregation, the activity enhancement was not up to the expected level in many systems. For illustration, graphene addition increased the H_2 production rate (1.02 fold) from 195 µmol h^{-1} to 298 µmol h^{-1} with $Sr_2Ta_2O_7$ photocatalyst.[32] Likewise, the bare TiO_2 produced 5 µmol h^{-1} of H_2 while the loading of rGO

15 increased that to 20 µmol h^{-1}.[33] On the other hand, in some other cases, the activity was inadequate even after loading of graphene. Nanocomposites of TiO_2 (Degussa P25) supported over hydrothermally reduced GO produced 75 µmol h^{-1} of H_2 under UV light irradiation.[34] TiO_2-MoS_2/graphene was used as an UV

20 active catalyst and the H_2 generation was found to be 165 µmol h^{-1}. GO wrapped amine functionalized TiO_2 was used for the production of 0.8 µmol h^{-1} of H_2.[35] Li *et al.* demonstrated photocatalytic H_2 production using TiO_2 decorated over graphene nanosheets which in turn generated 160 µmol h^{-1} g$_{cat}^{-1}$ of H_2.[36]

25 Clearly, considerable improvements in terms of activity are necessary to fully exploit graphene based photocatalysts in water splitting. Herein, we report Cu_2O-TiO_2/rGO photocatalyst with phenomenal water splitting ability. To the best of our knowledge this is the highest H_2 production rate reported so far using a

30 graphene supported photocatalytic system and also it is worth to mention here that ~7 fold enhancement was observed with the loading of rGO.

Results and Discussion

Powder X-ray diffraction

35 The phase purity and crystallinity of the synthesized photocatalysts (TiO_2 NPS and Cu_2O-TiO_2/rGO) was investigated using powder X-ray diffractometer, as shown in Fig. 1. The phase pure anatase TiO_2 NPs (calcined at 400 ℃ for 2 h) was literally matched with the JCPDS card number 21-1272.[37] But a

40 significant change in anatase phase TiO_2 took place after it calcined at a higher temperature (500 ℃ for 5 h) during the synthesis of Cu_2O-TiO_2/rGO photocatalyst. The additional peaks at 2θ angles of 27.61, 35.68, 41.48, 44.32 and 56.75º in Cu_2O-TiO_2/rGO corresponds to the (110), (101), (111), (210) and (110)

45 plans of rutile TiO_2 (JCPDS card number is 89-0555). It is widely known that the particular proportion of mixed phase TiO_2 (anatase and rutile, P-25 TiO_2 as an example) has always showed better photocatalytic performance rather than individual faceted TiO_2.[38] The weight percentage ratio of anatase to rutile phase

50 according to peak area [with respect to the (101) plane at 2θ=25.52º of anatase phase and (110) plane at 2θ=27.61º of rutile phase] was found to be ~74:26 which is an advantage of the present photocatalyst for the enhanced performance. This anatase and rutile ratio is almost similar to P-25 Degussa TiO_2 as a bench

55 mark commercially available photocatalysts. Further the decrease in peak width as compared to the pristine TiO_2 NPs inferred the crystalline nature of the Cu_2O-TiO_2/rGO photocatalyst. Besides, the diffractogram of Cu_2O-TiO_2/rGO

exhibited the peaks at the angles of 29.58, 36.23, 42.52, 52.60,

60 59.66, 73.35 and 77.79 accorded to the (110), (111), (200), (211), (220), (311) and (222) planes which confirmed the presence of Cu_2O (JCPDS card number is 77-0199).[39] This provides clear evidence for the reduction of copper precursor during ultrasound irradiation, from Cu^{2+} to Cu^+ (Cu_2O).
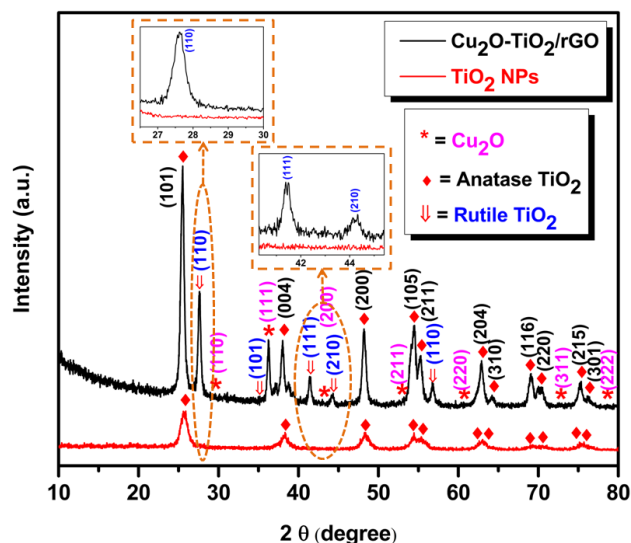
65 **Fig. 1** Powder X-ray diffraction patterns of pristine TiO_2 NPs and Cu_2O-TiO_2/rGO photocatalysts.

UV-vis diffuse reflectance spectra

The UV-vis absorbance spectra recorded in diffuse reflectance mode and Tauc's plots of TiO_2 NPs, Cu_2O-TiO_2 nanocomposite

70 and Cu_2O-TiO_2/rGO photocatalyst are depicted in Fig. 2. It is clearly seen from Fig. 2a that the absorption edge of pure TiO_2 NPs is at 386 nm corresponding to the band gap energy of 3.21 eV (Fig. 2b), whereas the band gap energy for Cu_2O loaded TiO_2 NPs is at 2.87 eV. The red shift of absorption edge from 386 nm

75 (for TiO_2 NPs) to 431 nm (for Cu_2O-TiO_2) is due to the Cu_2O. But addition of rGO had no effect on the absorption edge which is expected because rGO serves as a high carrier migrant solid support for the Cu_2O-TiO_2 nanocomposite. In addition, a shoulder in the absorption spectra was observed for both Cu_2O-TiO_2 and

80 Cu_2O-TiO_2/rGO which is due to interface charge transfer (IFCT) from TiO_2 valance band (VB) to Cu_2O and can be found around 450 nm.[40] The DRS results clearly demonstrate that Cu_2O loading shifts the absorption edge of TiO_2 NPs into the visible region, which in turn decreases the band gap energy and thereby

85 improves and extends the photo-absorption and photocatalytic performance of TiO_2 NPs into the visible region.
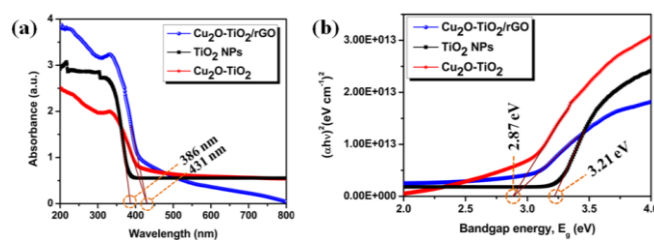
Fig. 2 (a) UV-vis absorbance (recorded in DRS mode) spectra and (b) Tauc plots of TiO_2 NPs, Cu_2O-TiO_2 and Cu_2O-TiO_2/rGO.

SEM-EDS

To study the surface morphology and to determine the weight percentage of Cu and Ti in the Cu_2O-TiO_2/rGO photocatalyst, field emission – scanning electron microscope (FE-SEM) and
5 energy dispersive spectroscopy (EDS) analysis were performed (Fig. 3). A homogeneous distribution with almost spherical shaped Cu_2O-TiO_2 nanocomposites can be seen from the SEM images, as depicted in Fig. 3a. The purity of Cu_2O-TiO_2/rGO photocatalyst is confirmed by EDS analysis (Fig. 3b) and the
10 corresponding wt% results are listed in the table (inset of Fig. 3b).
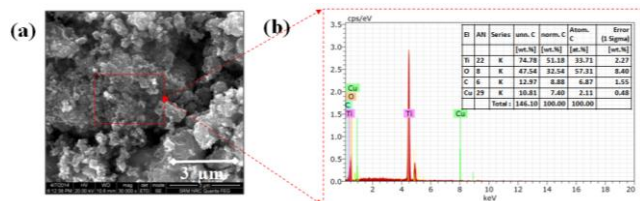
Fig. 3 (a) SEM image of Cu_2O-TiO_2/rGO and (b) EDS spectrum [inset: Wt% table].

TEM

Further confirmation of particle size and uniform distribution of
15 Cu_2O-TiO_2 nanocomposites over rGO layer was investigated using transmission electron microscopy (TEM) analysis, as shown in Fig. 4. As seen from the TEM images (Fig. 4a and 4b), very small and well dispersed Cu_2O-TiO_2 were anchored tightly onto the surface of rGO layer. The histogram of Cu_2O-TiO_2 (inset
20 of Fig. 4b) demonstrates that the Cu_2O-TiO_2 nanocomposites have a fairly broad size distribution ranging from 13 to 21 nm with a peak centered at ca. 16.1 nm. In addition, the crystalline structure of Cu_2O-TiO_2 is noticed clearly in Fig. 4. Furthermore, no free Cu_2O-TiO_2 was found in the background of the TEM
25 images (apart from the rGO layer), which confirmed the complete utilization of Cu_2O-TiO_2 nanocomposites.
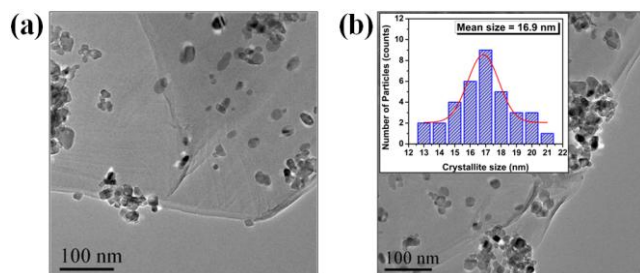
Fig. 4 (a) and (b) TEM images of Cu_2O-TiO_2/rGO [inset particle size distribution graph].

30 ## XPS

XPS analysis was also used to determine the chemical oxidation states of Cu and Ti, and also to analyze the existing oxygen functionalities. Fig. 5a shows the overall spectrum of the catalysts. The presence of peaks at around 284-291, 529-535, 930-960 and
35 455-468 eV in the overall survey spectrum are due to C 1s, O 1s, Cu 2p and Ti 2p, respectively. Gil et al. reported that the oxygen functional groups (epoxy groups) on graphene oxide act as effective nucleation centers for metal NPs that assist

homogeneous decoration as well as improved anchoring of metal
40 NPs on graphene oxide sheets.[41] In the present study, the presence of oxygen functional groups on GO results in the homogeneous dispersion as well as better adhesion of Cu_2O-TiO_2 nanocomposites on GO layer (Fig. 4a and 4b).
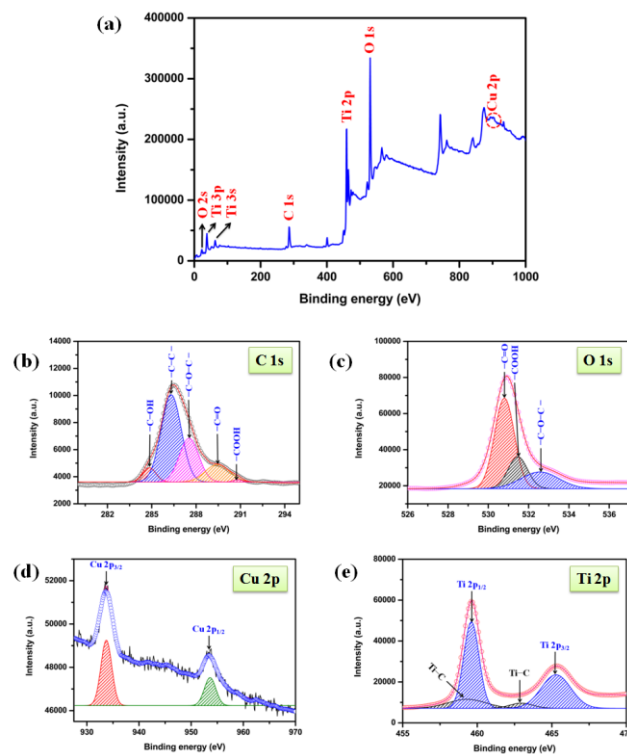
45 **Fig. 5** XPS spectra of the Cu_2O-TiO_2/rGO: (a) XPS survey spectrum, (b) high resolution C 1s spectrum, (c) high resolution O 1s spectrum, (d) high resolution Cu 2p spectrum and (e) high resolution Ti 2p spectrum.

The –COOH groups facilitate the linkage Cu_2O-TiO_2
50 nanocomposites on GO layer by replacing the proton of – COOH.[42] But on the other hand, the oxygen functionalities retard the carrier mobility of graphene and thereby reduce the photocatalytic activity. Hence it is essential to reduce the oxygen functional groups at-least to an extent following exfoliation or
55 after loading the metal NPs over the graphene layer. High resolution C 1s and O 1s XPS spectra gave an unambiguous picture about the existing oxygen functional groups in the graphene layer of Cu_2O-TiO_2/rGO photocatalyst. For instance, the broad peak of high resolution C 1s spectrum was
60 deconvoluted to five peaks that endorsed the presence of C−OH, C−C, C−O−C, C=O and –COOH (Fig. 5b).[43] Utmost reduction of C−OH, C=O and –COOH groups was presumed by considering the meager intense peaks centered at 284.8, 289.4 and 290.8 eV respectively. It was further confirmed by the deconvolution of O
65 1s spectrum which showed only three peaks that devoted to C=O, –COOH and C−O−C functionalities (Fig. 5c).[44] The binding energy values of C=O and Cu−O are almost equal and hence the merged broad peak was observed at 530.8 eV. Similarly the peak at 531.4 eV was attributed to the residual –COOH and Ti−O.[45]

Similarly, the high resolution Cu 2p region showed two major peaks at 933.7 and 953.5 eV which attributed to the Cu $2p_{3/2}$ and Cu $2p_{1/2}$ respectively.[46] Shake-up satellite peaks are the characteristics for metallic Cu(0) or Cu^{2+} (CuO) because of its d^9 configuration in the ground state. Whereas in the case of Cu^+ (Cu_2O), the d shell is completely filled (d^{10}) and hence the screening *via* a charge transfer into the d states is not possible, so the satellite peaks were absent for Cu_2O. The absence of shake-up satellite peaks in Cu 2p region clearly validated the existence of Cu_2O which is obtained by the sonochemical reduction of $Cu(NO_3)_2.3H_2O$ precursor (Fig. 5d).[47] Likewise, the high resolution Ti 2p spectrum showed two peaks centered at 459.6 and 465.3 eV which are due to Ti $2p_{1/2}$ and Ti $2p_{3/2}$ respectively. It is noteworthy that the values exactly matched with the literatures and substantiated the presence of TiO_2.[48] Two more additional weak peaks were observed at 459.1 and 463.0 eV which accorded with the Ti−C bond that authenticated the strong adhesion of TiO_2 over rGO surface (Fig. 5e).

Photoluminescence Studies
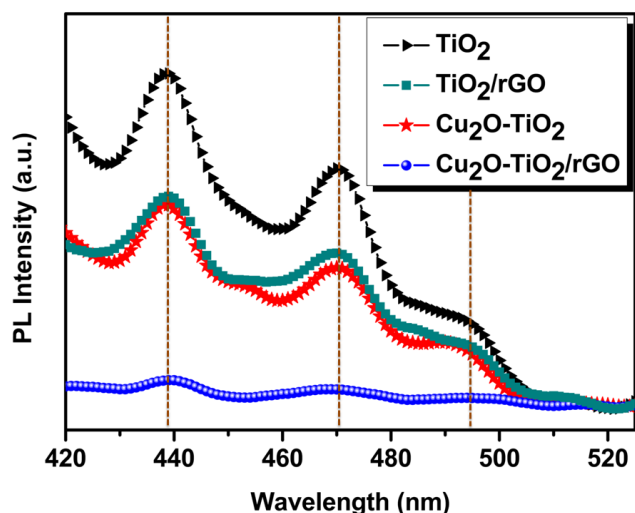
Fig. 6 Photoluminescence spectra of TiO_2, TiO_2/rGO, Cu_2O-TiO_2 and Cu_2O-TiO_2/rGO.

The shift in absorption edge of Cu_2O-TiO_2 compared to bare TiO_2 in the UV-vis diffuse reflectance spectra have already confirmed the formation of Cu_2O-TiO_2 heterojunction. To address the effect of rGO in Cu_2O-TiO_2 heterojunction on electron–hole separation, photoluminescence spectra (PL) was employed especially to characterize the recombination probability of bare TiO_2, TiO_2/rGO, Cu_2O-TiO_2 and Cu_2O-TiO_2/rGO photocatalysts. PL spectra in the wavelength of 420–525 nm of these photocatalysts are displayed in Fig. 6. All the photocatalysts showed similar PL spectrum with three emission peaks located at 438, 471 and 494 nm. The PL peaks at 438 and 471 nm are owing to the band edge free excitons.[49] Similarly the excitonic PL signal centered at 494 nm is directly related to surface oxygen vacancies or defects in the photocatalysts.[50] Very importantly, the luminescence intensities of TiO_2/rGO and Cu_2O-TiO_2 photocatalysts were lower than that of pristine TiO_2, which confirmed the lower electron–hole recombination probability in TiO_2/rGO and Cu_2O-TiO_2 photocatalysts. This unveiled that rGO slow down the

electron-hole pair recombination in TiO_2/rGO photocatalyst. In particular, because of the electric field associated with Cu_2O–TiO_2 nanocomposties, the electrons and holes were separated by the p–n junctions that resulted in decrease of PL intensity in Cu_2O–TiO_2 photocatalyst.[51] But more interestingly, almost negligible luminescence intensity was observed with rGO loaded Cu_2O–TiO_2 photocatalyst which inferred that rGO speedup the carrier mobility at the Cu_2O–TiO_2 p–n heterojunctions. This observation implied its high efficiency in electron–hole separation and hence increased photocatalytic activity. Combining the UV-vis DRS results (Fig. 2), the PL studies further confirmed the formation of heterojunctions between TiO_2 and Cu_2O and also disclosed that rGO delayed or almost prevent the electron-hole pair recombination.

Photoluminescence Studies

To understand the influence of electron storing, transferring and shuttling assets of rGO at the interfacial Cu_2O doped TiO_2 p-n hetero-junction, photoelectrical response of TiO_2, Cu_2O-TiO_2 and Cu_2O-TiO_2/rGO were studied (Fig. 7). It is clearly evident from the photocurrent measurements that the Cu_2O-TiO_2/rGO generates higher photocurrent than that of bare TiO_2 and Cu_2O-TiO_2. The photocurrent enhancement of Cu_2O-TiO_2/rGO photocatalyst confirmed the prevention of charge carriers (electron-hole pair) recombination. The stable photocurrent generated with Cu_2O-TiO_2/rGO photocatalyst further endorsed that rGO act as a potent carrier mobile layer at the Cu_2O and TiO_2 heterojunction.
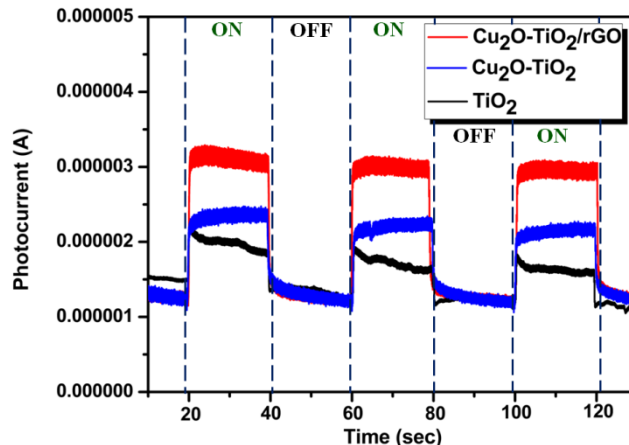
Fig. 7 Photoelectrochemical studies of TiO_2, TiO_2/rGO, Cu_2O-TiO_2 and Cu_2O-TiO_2/rGO.

Photocatalytic H_2 Production

In order to understand the specific role of individual components (TiO_2, Cu_2O and rGO) of the proposed photocatalyst, different photocatalysts were tested under identical condition towards the H_2 evolution, as depicted in Fig. 8. The relative order of photocatalytic activity for water splitting was Cu_2O/rGO (5060 μmol h^{-1} g_{cat}^{-1}) < TiO_2 NPs (7786 μmol h^{-1} g_{cat}^{-1}) < TiO_2/rGO (8226 μmol h^{-1} g_{cat}^{-1}) < Cu_2O-TiO_2 (16656 μmol h^{-1} g_{cat}^{-1}) < Cu_2O-TiO_2/rGO (110968 μmol h^{-1} g_{cat}^{-1}). The results obviously revealed that the activities of the pristine TiO_2 NPs, rGO loaded TiO_2 and rGO loaded Cu_2O were inadequate. However, the

presence of co-catalyst (Cu_2O) along with TiO_2 NPs showed comparable activity to some extent. Nevertheless the combination of all the three components was necessary to achieve enhanced activity. Indeed, the effect of rGO on the photocatalyst activity

5 was phenomenal which increased the H_2 evolution to approximately 94312 µmol h^{-1} g_{cat}^{-1}, *i.e.* from 16656 µmol h^{-1} g_{cat}^{-1} (for Cu_2O-TiO_2) to 110968 µmol h^{-1} g_{cat}^{-1} (for Cu_2O-TiO_2/rGO). In comparison with recently reported Cu_2O-TiO_2 photocatalyst which produced 18000 µmol h^{-1} g_{cat}^{-1} of H_2,[52] the

10 present photocatalytic system performed in presence of Cu_2O-TiO_2/rGO photocatalyst exhibited more than 6 fold enhancement.

Fig. 8 Splitting of water using different photocatalysts.

Effect of co-catalyst

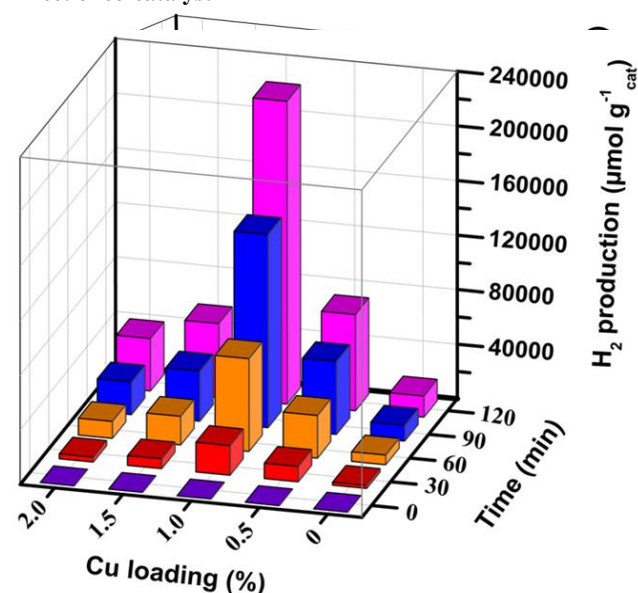**Fig. 9** Effect of Cu loading.

15 The previous experimental results clearly prove that the presence of all the three constituents (Cu_2O, TiO_2 and rGO) are necessary to attain superior H_2 production. Hence it is very important to optimize the Cu and GO loading. In order to understand the effect of co-catalyst loading, a series of experiments were carried out

20 with different Cu loaded (0, 0.5, 1.0, 1.5 and 2.0) photocatalysts and 3% GO loading was kept constant. Absence of co-catalyst, *i.e.* without Cu loaded catalyst (TiO_2/rGO) generated only meager
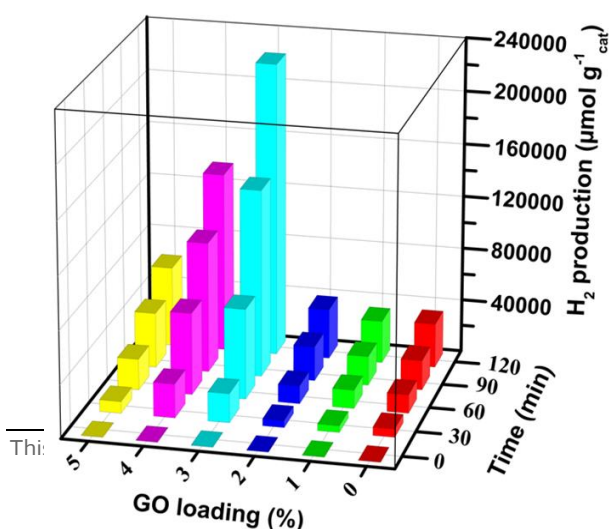
amount of H_2 (8226 µmol h^{-1} g_{cat}^{-1}) which was slightly higher than the pristine TiO_2 NPs (7786 µmol h^{-1} g_{cat}^{-1}). But the

25 introduction of Cu_2O increased the activity of the photocatalyst. Cu loading was systematically varied in the catalyst and the corresponding H_2 production rates were measured. The results are shown in Fig. 9. The optimum Cu loading was found to be 1.0 wt%.

30 **Effect of GO loading**

As can be seen from the catalyst optimization results, the role of rGO is very crucial. A ~7 fold increase in H_2 production was observed following the addition of rGO *i.e.* from 16656 (for Cu_2O-TiO_2) to 110968 µmol h^{-1} g_{cat}^{-1} (for Cu_2O-TiO_2/rGO). The

35 photoluminescence spectra inferred that presence of rGO prevents the electron-hole pair recombination and hence lowest emission intensity was identified with Cu_2O-TiO_2/rGO photocatalyst (Fig. 6). Optimization of the GO loading was also carried out by varying the GO loading from 0-5% with the optimized Cu loaded

40 (1.0%) photocatalyst. These results are shown in Fig. 10. The maximum H_2 evolution rate was obtained with 3 wt% rGO loaded catalyst. Any further increase of rGO loading decreased the H_2 production which might be attributable to the trade-off between the excellent charge transfer capability of rGO and its detrimental

45 effect on light absorption. Since the Cu_2O-TiO_2/rGO photocatalyst with 1.0% Cu and 3% GO loading showed maximum H_2 production efficiency, it was noted as an optimized photocatalyst for the splitting of water to produce H_2 under the present reaction condition.

50 **Fig. 10** Optimization of GO loading.

Plausible Mechanism

Based on the observations, and potential energy location of CB and VB of TiO_2 and the energy of CB and VB of Cu_2O, a tentative mechanism for the H_2 production using Cu_2O-TiO_2/rGO

55 photocatalyst is shown in Fig. 11.[53] The energy of CB of TiO_2 is lower than that of the CB of Cu_2O, so that the former acts as a sink for the photogenerated electrons following illumination of Cu_2O since the holes move in the opposite direction from the electrons, the photogenerated holes are trapped within the Cu_2O

60 making charge separation more efficient.[54] This is supported by the photoluminescence studies that the emission intensity of Cu_2O loaded TiO_2 was much lower than that of pristine TiO_2 (Fig. 6). The electron transfer to the CB of TiO_2 is mediated *via* rGO surface and these electrons are subsequently involved in the

65 reduction of proton (H^+) to produce H_2. At the same time, the h^+ trapped on the surface of the Cu_2O are scavenged by glycerol (a well known h^+ scavenger) present in the reaction medium to produce H^+ which in turn undergoes reduction with the photo-excited electron to produce H_2.[55]
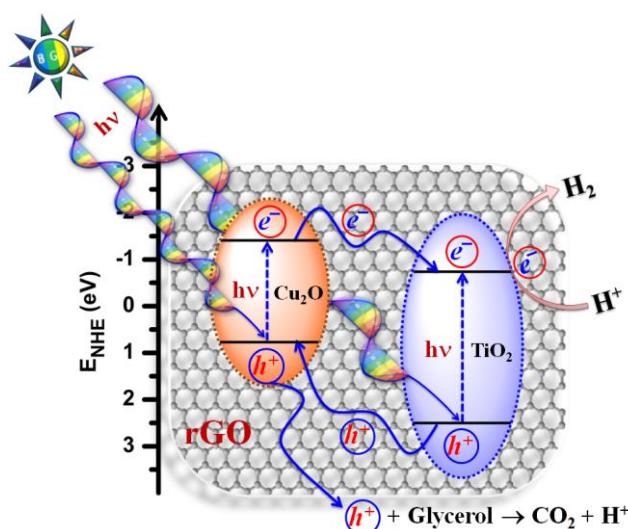
Cu_2O-TiO_2/rGO photocatalyst also exist as mixed phases of anatase and rutile with a ratio of ~74:26. The combination of Cu_2O, mixed phase TiO_2 and few layered rGO support r enhances the photoreactivity of Cu_2O-TiO_2/rGO significantly towards H_2 evolution from water. The effect of rGO in the present photocatalytic system is phenomenal which enhances the H_2 generation rate from 16656 μmol h^{-1} g$_{cat}^{-1}$ (for Cu_2O-TiO_2) to 110968 μmol h^{-1} g$_{cat}^{-1}$ (for Cu_2O-TiO_2/rGO) i.e. approximately 7 fold enrichment. More importantly, the catalyst can be recycled for at least four times without a significant loss in its activity.

Experimental Section

Materials

Titanium tetraisopropoxide (TTIP) and glycerol were purchased from Merck India Pvt Ltd. Graphite powder (synthetic, conducting grade, 325 mesh, 99.9995%) was from Alfa Aesar. $Cu(NO_3)_2.3H_2O$ was procured from Loba Chemie Pvt. Ltd. All the other chemicals such as $NaNO_3$, $KMnO_4$, H_2SO_4 and solvents were used as received from Rankem, India without further purification.

Preparation of GO and TiO_2 NPs

Graphene oxide (GO) was prepared from graphite powder using $NaNO_3$, $KMnO_4$ and H_2SO_4 by modified Hummers' method.[56] TiO_2 NPs was synthesized by hydrolysis and peptization of TTIP solution.[57] In detail, a 250 mL solution of distilled water with pH=3 (adjusted by adding HNO_3) was used as the hydrolysis catalyst. Hydrolysis of TTIP offered a turbid solution which was heated up to 60–70 ℃ for 20 h (peptization). After peptization process, the volume of the solution was reduced to 50 cm^3 and a white suspension was produced. The prepared precipitates were washed with ethanol and dried for 3 h at 100 ℃, a yellow-white powder was obtained and then it was calcined at 400 ℃ for 2 h to obtain TiO_2 NPs.

Preparation of Cu_2O-TiO_2/rGO

Cu_2O-TiO_2/rGO photocatalyst was prepared by ultrasonic reduction followed by wet impregnation method.[55] TiO_2 NPs along with different GO loading (0, 1, 2, 3, 4 and 5 wt%) were dispersed into an appropriate concentration of aqueous solution of $Cu(NO_3)_2\cdot3H_2O$ (0, 0.5, 1, 1.5 and 2 wt% of Cu). Then the solution was ultrasonicated for 1 h (low frequency ultrasonic horn operating at 20 kHz from SONICS, Vibra cell, USA). Then the mixture was pre-dried over a hot plate until complete evaporation of water and the resultant powder was dried in an oven at 80 ℃ for 12 h and then calcined at 500 ℃ for 5 h.

Characterization Techniques

X-Ray diffraction (XRD) studies were carried out using PANaltical X'pert powder diffractometer using Cu Kα radiation with an angular range of 10 to 80 º to identify the crystal structure and phases of TiO_2 and Cu_2O in the Cu_2O-TiO_2/rGO photocatalyst. Band gap of the prepared photocatalysts were determined using UV-vis DRS technique using Shimadhzu UV-2600 UV-vis spectrophotometer with a DRS mode. The chemical oxidation state of Ti and Cu, and the existing oxygen functionalities of rGO were examined using X-ray photoelectron spectroscopy (XPS) recorded in a Kratos Axis-Ultra DLD spectrometer with Mg-Kα radiation. The surface morphology and weight percentage of Cu and Ti in Cu_2O-TiO_2/rGO photocatalyst were confirmed by SEM-EDS analysis (FEI Quanta FEG 200 HR-SEM) which operated at 20 kV. JEM-2100 JEOL, Japan, transmission electron microscopy (TEM) with an accelerating

Fig. 11 Proposed mechanism for the Cu_2O-TiO_2/rGO-catalyzed water splitting reaction.

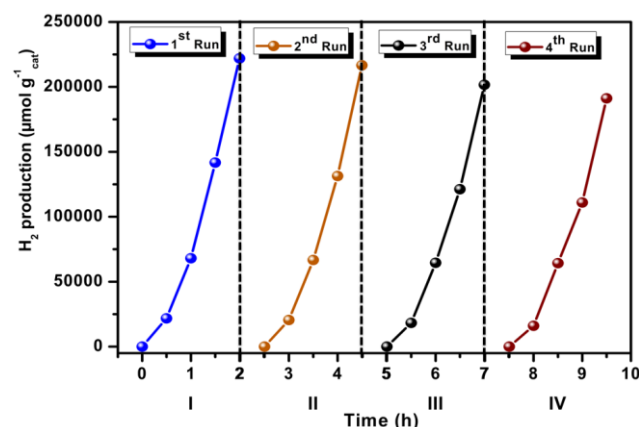**Fig. 12** Reusability of the Cu_2O-TiO_2/rGO photocatalyst in four successive experimental runs for the photocatalytic water splitting.

In addition to efficiency, sustainability / durability and recyclability are very important for commercial applications of the photocatalyst. To evaluate this, recyclability tests were carried out by evacuating the produced gases at regular intervals for the next cycle and the results are depicted in Fig. 12. A constant and similar H_2 production rate was observed for four cycles. The results revealed that the Cu_2O-TiO_2/rGO photocatalyst can be effectively recycled at least for four times without an apparent decrease in its photocatalytic activity, which clearly illustrated its high stability.

Conclusions

In summary, Cu_2O-TiO_2 nanocomposites over rGO layers are successfully fabricated by simple sonoreduction and subsequent wet impregnation method. The doping of Cu_2O enhances the photocatalytic activity by reducing the band gap energy to the visible light region. Likewise, the loading of rGO prolongs the lifetime of the photo-generated electron–hole pairs. As in commercial Degussa P25-TiO_2, the TiO_2 NPs in the present

voltage of 120 kV was used to analyze the particle size and size distribution of Cu_2O-TiO_2 particles over rGO layer. Image-J software was used to determine size distribution of particles.

Photoelectrochemical studies

Conventional three electrode configuration with a Pt-wire as counter electrode and Ag/AgCl (in saturated KCl) as a reference electrode was used to carry out the photoelectrochemical measurements. Photoelectrochemical data were recorded in a CHI608E electrochemical workstation. A light source of 250 W Xe arc lamp (OSRAM, Germany) was used for photocurrent measurements. A 0.1 M Na_2SO_4 aqueous solution was used as the electrolyte. The working electrode was prepared by mixing the 50 mg of photocatalyst with 150 mL of PEG (mol. wt 400) and 125 mL of ethanol was used to make slurry. Then it was coated on a 2.5×2.5 cm^2 fluorine-doped tin oxide (FTO) glass substrate with an active area of about 1×1 cm^2 by doctor-blade method using scotch tape as spacer. It was dried in air and then annealed at 350 ℃ for 45 min.

Reactor set-up and analysis methods for water splitting

In a typical procedure, 0.1 mg per mL of Cu_2O-TiO_2/rGO photocatalyst was dispersed in of 5% aqueous glycerol solution taken in a quartz reactor vessel. The mixture was magnetically stirred in the dark condition for 30 min and then evacuated for 30 min followed by 30 min N_2 purging for the complete removal of dissolved oxygen. Then it was illuminated under the lamp (Philips HPL-N-250W lamp) and the generated gas was collected at the given interval of time for analysis using an off-line gas chromatograph with TCD detector (Shimadzu GC-2014 with Molecular Sieve/5Å column) using N_2 as a carrier gas.

Acknowledgements

Notes and references

^{a} SRM Research Institute, SRM University, Kattankulathur 603203, Chennai, Tamilnadu, India; E-mail: neppolian.b@res.srmuniv.ac.in (B. Neppolian)

^{b} Nano Catalysis and Solar Fuels Research Laboratory, Department of Materials Science & Nanotechnology, Yogi Vemana University, Kadapa 516003, Andhra Pradesh, India

^{c} National Taiwan University of Science and Technology, Taipei 106-07, Taiwan

^{d} Department of Chemistry, North Carolina Central University, Durham, NC 27707, USA; E-mail: kvinodg@nccu.edu (K. Vinodgopal)

1   M. S. Dresselhaus and I. L. Thomas, *Nature,* 2001, **414**, 332.
2   P. V. Kamat, *J. Phys. Chem. C,* 2007, **111**, 2834.
3   D. Tilman, J. Hill and C. Lehman, *Science*, 2006, **314**, 1598.
4   P. V. Kamat, *J. Phys. Chem. Lett.,* 2011, **2**, 242.
5   J. A. Turner, *Science,* 1999, **285**, 687.
6   J. O. Bockris, *Int. J. Hydrogen Energ.,* 2002, **27**, 731.
7   G. Girishkumar, M. Rettker, R. Underhile, D. Binz, K. Vinodgopal, P. McGinn and P. V. Kamat, *Langmuir,* 2005, **21**, 8487.
8   H. J. Kim, S. H. Lee, A. A. Upadhye, I. Ro, M. I. Tejedor-Tejedor, M. A. Anderson, W. B. Kim and G. W. Huber, *ACS Nano,* 2014, **8**, 10756.
9   S. Shen, C. X. Kronawitter, J. Jiang, P. Guo, L. Guo and S. S. Mao, *Nano Energy,* **2013**, 2, 958.
10   D. Ravelli, D. Dondi, M. Fagnoni and A. Albini, *Chem. Soc. Rev.,* 2009, **38**, 1999.
11   A. Fujishima, and K. Honda, *Nature,* 1972, **238**, 37.
12   H. Pann, and Y. –W. Zhang, *Nano Energy,* 2012, **1**, 488.
13   B. Neppolian, H. C. Choi, S. Sakthivel, B. Arabindoo and V. Murugesan, *J. Hazard. Mater.,* 2002, **89**, 303.
14   H. Yamashita, M. Harada, J. Misaka, M. Takeuchi, B. Neppolian and M. Anpo, *Catal. Today,* 2003, **84**, 191.
15   A. Kudo and Y. Misekia, *Chem. Soc. Rev.,* 2009, **38**, 253.
16   Y. Inoue, *Energy Environ. Sci.,* 2009, **2**, 364.
17   H. Tuysuz and C. K. Chan, *Nano Energy,* 2013, **2**, 116.
18   M. Ni, M. K. H. Leung, D. Y. C. Leung and K. Sumathy, *Renew. Sust. Energ. Rev.,* 2007, **11**, 401.
19   P. A. Mangrulkar, V. Polshettiwar, N. K. Labhsetwar, R. S. Varma and S. S. Rayalu, *Nanoscale,* 2012, **4**, 5202.
20   T. Zhang, K. Zhao, J. Yu, J. Jin, Y. Qi, H. Li, X. Hou and G. Liu, *Nanoscale,* 2013, **5**, 8375.
21   H. Kato , K. Asakura and A. Kudo, *J. Am. Chem. Soc.,* 2003, **125**, 3082.
22   M. Hara, T. Kondo, M. Komoda, S. Ikeda, K. Shinohara, A. Tanaka, J. N. Kondoa and K. Domen, *Chem. Commun.,* 1998, 357.
23   K. Maeda, T. Takata, M. Hara, N. Saito, Y. Inoue, H. Kobayashi and K. Domen, *J. Am. Chem. Soc.,* 2005, **127**, 8286.
24   J. S. Lee, *Catal. Surv. Asia,* 2005, **9**, 217.
25   A. Kudo, H. Kato and S. Nakagawa, *J. Phys. Chem. B,* 2000, **104**, 571.
26   A. Deshpande, P. Shah, R. S. Gholap and N. M. Gupta, *J. Colloid Interf. Sci.,* 2009, **333**, 263.
27   P. S. Lunawat, S. Senapati, R. Kumar and N. M. Gupta, *Int. J. Hydrogen Energ.,* 2007, **32**, 2784.
28   Q. Xiang, J. Yu and M. Jaroniec, *Nanoscale,* 2011, **3**, 3670.
29   X. –J. Lv, S. –X. Zhou, C. Zhang, H. –X. Chang, Y. Chen and W. –F. Fu, *J. Mater. Chem.,* 2012, **22**, 18542.
30   P. Wang, N. M. Dimitrijevic, A. Y. Chang, R. D. Schaller, Y. Liu, T. Rajh and E. A. Rozhkova, *ACS Nano,* 2014, **8**, 7995.
31   L. Jia, D. –H. Wang, Y. –X. Huang, A. –W. Xu and H. –Q. Yu, *J. Phys. Chem. C,* 2011, **115**, 11466.
32   A. Mukherji, B. Seger, G. Q. Lu and L. Wang, *ACS Nano,* 2011, **5**, 3483.
33   J. Shen, M. Shi, B. Yan, H. Ma, N. Li and M. Ye, *Nano Res.,* 2011, **4**, 795.
34   W. Fan, Q. Lai, Q. Zhang and Y. Wang, *J. Phys. Chem. C,* 2011, **115**, 10694.
35   Q. Xiang, J. Yu and M. Jaroniec, *J. Am. Chem. Soc.,* 2012, **134**, 6575.
36   N. Li, G. Liu, C. Zhen, F. Li, L. Zhang, L. and H. –M. Cheng, *Adv. Funct. Mater.,* 2011, **21**, 1717.
37   B. Neppolian, Q. Wang, H. Yamashita and H. Choi, *Appl. Catal. A: Gen.,* 2007, **333**, 264.
38   D. C. Hurum, A. G. Agrios and K. A. Gray, *J. Phys. Chem. B,* 2003, **107**, 4545.
39   T. Jiang, T. Xie, L. Chen, Z. Fu and D. Wang, *Nanoscale,* 2013, **5**, 2938.
40   H. Irie, S. Miura, K. Kamiya and K. Hashimoto, *Chem. Phys. Lett.,* 2008, **457**, 202.
41   G. Gil, P. A. A. P. Marques, C. M. Granadeiro, H. I. S. Nogueira, M. K. Singh and J. Gracio, *Chem. Mater.,* 2009, **21**, 4796.
42   S. Shrestha, W. C. Choi, W. Song, Y. T. Kwon, S. P. Shrestha and C. Y. Park, *Carbon,* 2010, **48**, 54.
43   M. Gopiraman, S. G. Babu, Z. Khatri, K. Wei, M. Endo, R. Karvembu and I. S. Kim, *Catal. Sci. Technol.,* 2013, **3**, 1485.
44   M. Gopiraman, S. G. Babu, Z. Khatri, K. Wei, Y. A. Kim, M. Endo, R. Karvembu and I. S. Kim, *J. Phys. Chem. C,* 2013, **117**, 23582.
45   B. Chai, B. Peng, X. Zhang, J. Mao, K. Li and X. Zhang, *Dalton Trans.,* 2013, **42**, 3402.
46   S. G. Babu, N. Neelakandeswari, N. Dharmaraj, S. D. Jackson and R. Karvembu, *RSC Adv.,* 2013, **3**, 7774.
47   M. Gopiraman, S. G. Babu, Z. Khatri, K. Wei, Y. A. Kim, M. Endo, R. Karvembu and I. S. Kim, *Carbon,* 2013, **62**, 135.
48   G. M. An, W. H. Ma, Z. Y. Sun, Z. M. Liu, B. X. Han, S. D. Miao, Z. J. Miao and K. L. Ding, *Carbon,* 2007, **45**, 1795.

49 B. Liu, X. Wang, G. Cai, L. Wen, Y. Song and X. Zhao, *J. Hazard. Mater.,* 2009, **169**, 1112.

50 L. Jing, H. Fu, B. Wang, D. Wang, B. Xin, S. Li and J. Sun, *Appl. Catal. B: Environ.,* 2005, **62**, 282.

5 51 S. Chu, X. Zheng, F. Kong, G. Wu, L. Luo, Y. Guo, H. Liu, Y. Wang, H. Yu and Z. Zou, *Mater. Chem. Phys.,* 2011, **129**, 1184.

52 J. M. Valero, S. Obregon and G. Colon, *ACS Catal.,* 2014, **4**, 3320.

53 H. Xu, S. Ouyang, L. Liu, D. Wang, T. Kako and J. Ye, *Nanotechnology,* 2014, **25**, 165402.

10 54 L. Liu, X. Gu, C. Sun, H. Li, Y. Deng, F. Gao and L. Dong, *Nanoscale,* **2012**, *4*, 6351–6359.

55 D. P. Kumar, M. V. Shankar, M. M. Kumari, G. Sadanandam, B. Srinivas and V. Durgakumari, *Chem. Commun.,* 2013, **49**, 9443.

56 W. S. Hummers and R. E. Offeman, *J. Am. Chem. Soc.,* 1958, **80**, 1339.

15 57 S. Mahshid, M. S. Ghamsari, M. Askari, N. Afshar and S. Lahuti, *Quantum Electron. Optoelectron.,* 2006. **9**, 65.

Nanoscale Accepted Manuscript